ACS OMEGA

Open Access

http://pubs.acs.org/journal/acsodf

Article

Rational Design and Development of a Soluble Mesoporous Carrier for the Solidification of a Preconcentrated Self-Nanoemulsion Formulation

Ilham Kuncahyo, Ana Indrayati, and Syaiful Choiri*

Cite This: *ACS Omega* 2023, 8, 38676–38689

Read Online

ACCESS | Metrics & More | Article Recommendations | Supporting Information

ABSTRACT: The solidification of self-preconcentrated nanoemulsion without changes in nanodroplet formation gains particular consideration due to the interaction between solidified carriers. This work aimed to develop mannitol mesoporous as a soluble carrier for supersaturated self-nanoemulsion (SSNE) using a design of experiment (DoE) approach. The mesoporous carrier was prepared by a spray-drying technique. The type of templating agent (TA) used to form a porous system, the amount of TA, and solid loading in the spray-drying process were studied. Several characterizations were performed for mannitol mesoporous formation, namely, powder X-ray diffraction, thermal analysis, scanning electron microscopy, and surface area analyzer. Solidification of SSNE incorporated into the mesoporous mannitol was carried out, followed by compaction behavior, flowability, and nanodroplet formation. The results revealed several process parameters for preparing the mesoporous mannitol, notably TA, which gained more significant consideration. Solid loading in the mesoporous preparation system reduced the surface area and pore size and did not affect solid SSNE flowability. The amount of TA increased the pore size and volume dramatically as well as the compactibility and flowability. Ammonium carbonate was the preferable TA for preparing the mesoporous carrier, particularly for the nanodroplet formulation process. In addition, synergistic and antagonistic interactions between factors were also observed. The optimized mesoporous carrier was applied for solidification, and there was no difference between SSNE and solid SSNE in the performance of nanodroplet formation.

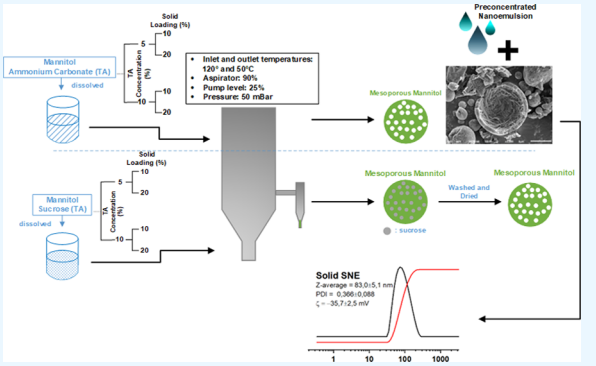

1. INTRODUCTION

Lipid-based formulation (LFB) is attractive to attain particular consideration for bioavailability enhancement. This formulation has been applied for two decades and has increased dramatically to date.[1,2] Among LBFs, self-nano emulsifying (SNE) formulation is preferable and promising as a primary choice owing to low energy processing and cost, high loading, and simple way compared with solid lipid nanoparticle or nano-structured lipid carrier.[1,3] SNE formulation comprising oil, surfactant, and cosurfactant forms nanodroplet when introduced and diluted with medium under gentle agitation. In addition, it depends on the oil and surfactant intermolecular interaction.[4] Not only lipophilic compounds but hydrophilic drugs can also be incorporated into SNE, for instance, macromolecules or proteins, by chemical modification of the drug structure using hydrophobic ion pairing or phospholipid complex.[5,6] The lymphatic pathway is one of the transport strategies for bioavailability enhancement by addressing the efflux problem in the gut.[7] In addition, the polymer can be incorporated to modify nanodroplet emulsion, namely, mucoadhesive properties[8] and ζ-potential changing system[9] against the mucus barrier in oral absorption.

Moreover, the SNE loading can be enhanced by high/saturated drug loading in order to achieve a high potency delivery system with low SNE formulation required, owing to the restriction of surfactant in chronic use. This formulation is known as supersaturated SNE (sSNE). However, precipitation of the drug during sSNE formulation dilution is the main problem.[10] However, the drawback of sSNE formulation appears owing to stability problems, portability, feasibility, and flexibility to formulate in simple preparation.[11] Therefore, the solidification of SSNE to achieve solid SSNE (s-SSNE) is the primary concern for addressing those issues.

The appropriate carrier for the solidification of SNE is a hidden hurdle. Carrier for sSNE can promote alteration of nanodroplet formation as well as the formation of micellar or phase separation owing to its interaction.[12,13] This interaction is

Received: August 12, 2023
Accepted: September 15, 2023
Published: October 2, 2023

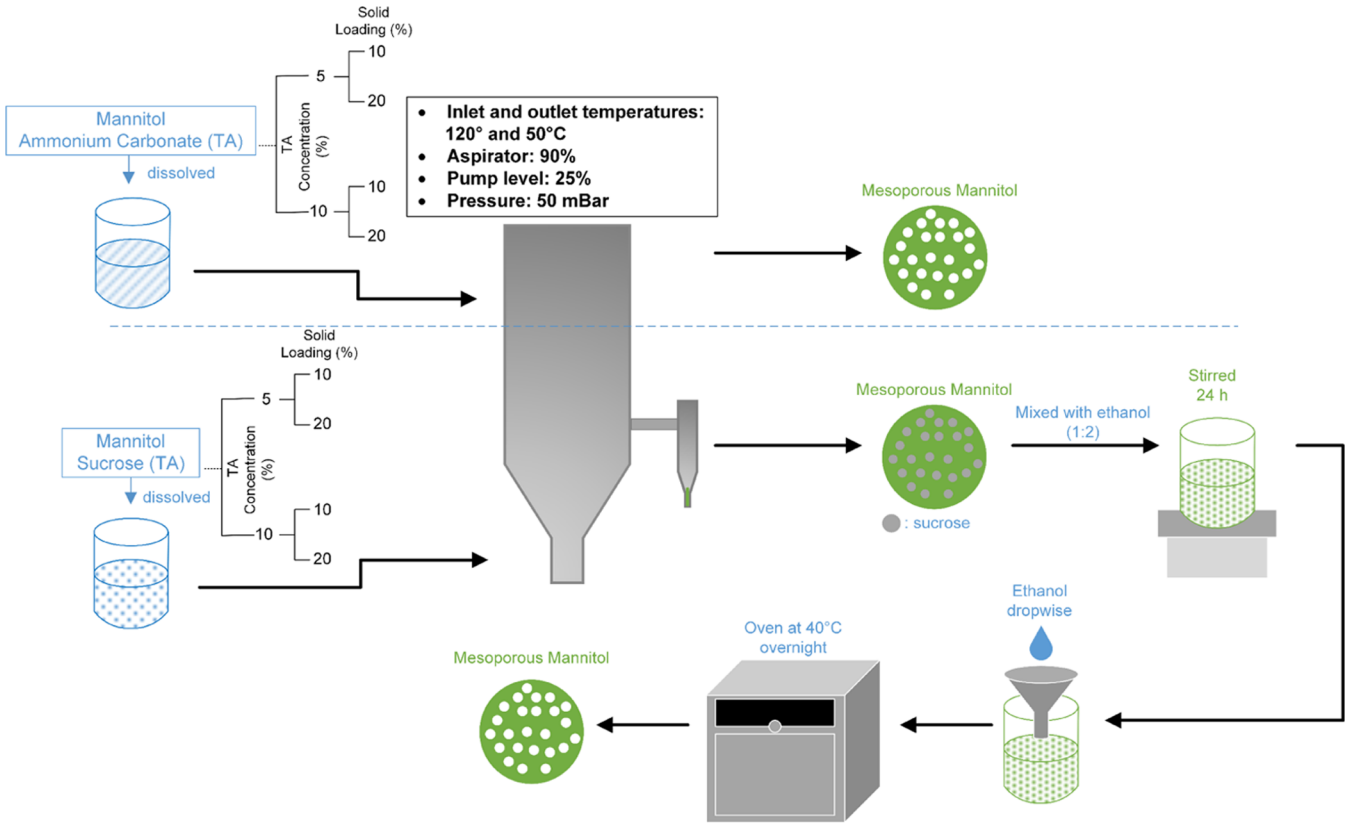

Figure 1. Mannitol mesoporous preparation scheme using different templating agents.

influenced by the hydrogen or hydrophobic, even ionic, interaction between SNE formulation and carrier. The carboxylate group on the fatty acid chain side of SNE components promotes interaction with the positive charge in the carrier through ionic interaction. A hydrogen bond interaction mediates the lower energy of interaction. Generally, a silica-based carrier was applied for the SNE solidification; however, a study reported that the interaction of the SNE component and the free silanol group in silica involves hydrogen bonding. This interaction influences the nanodroplet formulation during dilution. In contrast, the combination of nanodroplet and micellar formations might be observed during the dilution.[13,14] Therefore, silica is not recommended for the solidification of SNE.[12] Thus, a water-based and nonionic carrier is a potential candidate for the carrier of SNE. Solidification of SNE using spray-drying or freeze-drying technologies alters the spontaneous capability of SNE formulation due to solidifying the nanoemulsion droplet.[15] Spontaneous (self-emulsification) ability depends on the free energy due to dilution when surfactant and cosurfactant contribute to the mechanism. In addition, the carrier's fundamental role is the drug-to-carrier ratio. Both technologies require a considerable amount of carrier for solidification, producing a low drug loading.[11,13] Therefore, these technologies should be reconsidered.

Mannitol is a soluble sugar along with no hygroscopic characteristic, which can be modified physically or chemically as a carrier for SSNE.[16,17] Owing to the characteristic, it will be accessible to be incorporated into the carrier without any humid adsorbing onto the surface of the carrier.[12,18] However, several soluble and biocompatible materials, namely, lactose, can also be applied as carriers.[19] Physical modification through particle engineering increases the efficiency of SNE solidification due to the surface area required for absorption/adsorption of SNE into/on the carrier.[20] Either absorption or adsorption is very dependent on the carrier interaction. Generally, insoluble carriers, namely, silica, modified silica, and alumina−silica, involve an adsorption mechanism in which the liquid SNE is dispersed and adsorbed on the surface of the carrier.[11] Meanwhile, the soluble carriers, namely, mannitol, sucrose, lactose, and other sugars, involve an absorption mechanism. The performance of the absorption mechanism depends on the carrier's surface area. In addition, the interaction between soluble carriers and SNE formulation is also to be considered.[21] The larger the surface area, the more efficient the absorption process.[22] Moreover, the nanodroplet formation after dispersing the sSNE in the medium is affected by the interaction between the carrier and SNE formulation. There are three challenges: (1) formation of nanodroplet without changing its phase, (2) formation of the micellar system owing to oil interaction with the carrier, and (3) phase separation owing to different affinity of the interaction between components in SNE formulation with the carrier.[12]

Mesoporous material has a porous system of about 2−50 nm as a promising delivery carrier for sSSNE.[23,24] The presence of a porous system enhances the surface area, and then, the ability of the carrier to adsorb/absorb the liquid into/on the carrier is increased dramatically. However, the porous system depends on preparing a porous material that can be carried out through physical modification. For instance, the elimination of templating agents or pore-promoting agents is the primary consideration for producing the mesoporous system.[18] Pore formation behavior governs the ability of the solidification process.[11] Therefore, this should be investigated thoroughly. On the other hand, modification through a porous system might

https://doi.org/10.1021/acsomega.3c05948
ACS Omega 2023, 8, 38676−38689

alter the physicomechanical characteristics, namely, powder flow and compaction behavior.[20] Hence, the aim of this work was to develop mannitol mesopores using a factorial design approach as a simultaneous assessment and optimization process followed by loading of supersaturated self-nanoemulsion (SSNE) in order to obtain solid SSNE (sSSNE).

2. MATERIALS AND METHODS

2.1. Materials. SNE formulation consisted of Capryol-90 (Gattefose, France) as oil, Tween-80 (Sigma-Aldrich, St. Louis, MO) as a surfactant, and Transcutol P (Gattefose, Saint-Priest, France). Mannitol was obtained from Roquette (Lestrem, France), and sucrose and ammonium carbonate were obtained from Merck (Darmstadt, Germany). Ca-pitavastatin (PVT) as a lipophilic drug was used as a drug model in this study, and it was purchased from Thanen Chemical Co., Ltd. (Xinbei District, China).

2.2. Experimental Design for Developing Mannitol Mesoporous. The design and development of mannitol mesoporous carriers were performed by using a 2^3-factorial design. An 8-run was constructed according to the type of TA, the concentration of TA in total solid, and the amount of solid loading in a spray-drying solution, and those are determined by pore formation characteristics, flowability, and compactibility, as well as the nanodroplet formation. The design is presented in Table S1 (Supporting Information). The main effect, two-factor interactions, and three-factor interaction models were applied and analyzed by multiple linear regression analysis. Each model was fitted to the following equation

$$Y = \beta + a \times A + b \times B + c \times C + ab \times A \times B + ac \times A \times C + bc \times B \times C + abc \times A \times B \times C \quad (1)$$

where β is an intercept; a, b, and c are the coefficient regression of the main effect model; and ab, ac, and bc are the coefficient regression of two-factor interaction models. Meanwhile, A, B, and C are the levels of each factor, i.e., type of TA, concentration of TA, and solid loading. Each model was evaluated and validated using a statistical approach, ANOVA, with a confidence level of 95% ($p = 0.05$). The best model had the highest R^2, adjusted R^2, and predicted R^2 and the lowest predicted residual error sum of square (PRESS). The model should follow to be significant ($p < 0.05$). The model validation, according to a previously reported study,[25] was $R^2 > 0.7$, the difference between adjusted R^2 and predicted R^2 was also considered not more than 0.2, and adequate precision, i.e., signal-to-noise ratio, was more than 4. The surface plot was constructed according to the equation for the evaluation of further interaction.

2.3. Mannitol Mesoporous Preparation. The mesoporous mannitol was prepared by a spray-drying method. The scheme that illustrates the preparation of mannitol mesoporous is presented in Figure 1. Briefly, mannitol and TA, either ammonium carbonate or sucrose, were dissolved in water with total solid loading according to Table S1 (Supporting Data). The solution was dried using a Buchi mini spray dryer B-290 (Flawil, Switzerland). The spray dryer condition was inlet and outlet temperatures of 120 and 50 °C, respectively, aspirator of 90%, pump level of 25%, and pressure of 50 mbar. Elimination of TA, sucrose, in spray-dried sample was carried out by washing with ethanol. The spray-dried sample mannitol-sucrose was mixed with ethanol (1:2) and stirred for 24 h. Furthermore, the sample was filtered, and the retained sample was washed with ethanol dropwise. Thereafter, the sample was dried in an oven at 40 °C overnight. The solidified mannitol was collected and stored in the desiccator until further characterization and formulation. The mannitol-ammonium carbonate spray-dried sample was also directly stored without further treatments.

2.4. Thermal Analysis. The thermal behavior of the mannitol mesoporous was characterized using Shimadzu DSC-60 differential scanning calorimeter (DSC) and Shimadzu DTG-60 thermal gravimetric analyzer (TGA) (Kyoto, Japan). The temperature and enthalpy were calibrated using standard indium. An approximate 5 mg sample was placed into an Al_2O_3 (aluminum hermetic) pan and heated from 30 to 300 °C at 10 °C/min under a 30 mL/min nitrogen atmosphere. An empty pan was used as a reference. The thermal data, namely, enthalpy, melting point, transition, decomposition, and weight loss, were processed and analyzed using TA-60 v 2.21 (Shimadzu Corporation, Tokyo, Japan).

2.5. Powder X-ray Diffraction. Powder X-ray diffraction (PXRD) was performed to characterize the crystallinity of the spray-dried sample, depending on the diffraction angle (θ). The PXRD pattern was obtained using a Rigaku SmartLab X-ray diffractometer (The Woodlands, TX) with Cu Kα radiation (λ 1.5406 Å), a voltage of 40 kV, and a current of 30 mA. The sample was placed into a sample holder and scanned from 3 to 45° 2θ range at the rate of 3°/min with the step size of 0.02. The diffractogram was processed by using PDXL software (Rigaku, The Woodlands, TX).

2.6. Morphology Characterization. Morphology characterization of mannitol mesopores was performed using a JEOL JSM-6510LA scanning electron microscope (SEM) (Tokyo, Japan). Prior to evaluation, the sample was coated with platinum for 120 s using a JEOL JEC-3000PC auto fine coater (Tokyo, Japan). Samples were observed at an accelerating voltage of 5 kV by using several magnifications until the desired photograph was achieved.

2.7. Surface Area Analyzer. Specific surface area, pore volume, and pore size are characterized using a Quadrosorb Evo surface area analyzer (Boynton Beach, FL). Prior to analysis, the sample was vacuumed for 24 h. The measurement was carried out by using the nitrogen sorption−desorption technique. Specific surface area, pore volume, and pore size were calculated by using the Brunauer−Emmet−Teller (BET) equation and processed by using Quadrosorb software (Boynton Beach, FL).

2.8. Compaction Behavior. Compaction behavior was assessed by the compactibility of mannitol mesoporous and tensile strength. Briefly, 200 mg of mannitol mesoporous was weighed and manually filled into the tooling machine. Prior to compaction, the tooling wall was lubricated by using magnesium stearate. All spray-dried samples were compressed at a similar compression force, 5 kN. The tablet crushing strength was characterized by using a Stokes Monsanto hardness tester. The tablet's diameter (d) and height (h) were measured using a caliper. The tensile strength was calculated according to the following equation

$$\text{tensile strength} = \frac{2F}{d \cdot h} \quad (2)$$

2.9. Preparation and Incorporation of Supersaturable Self-Nanoemulsion. Optimized supersaturated self-nanoemulsion (SSNE) formulation consisting of 23.4% Capryol-90, 35.6% Tween-80, and 40% Transcutol P was obtained from a previous study incorporated into mesoporous carrier through

https://doi.org/10.1021/acsomega.3c05948
ACS Omega 2023, 8, 38676−38689

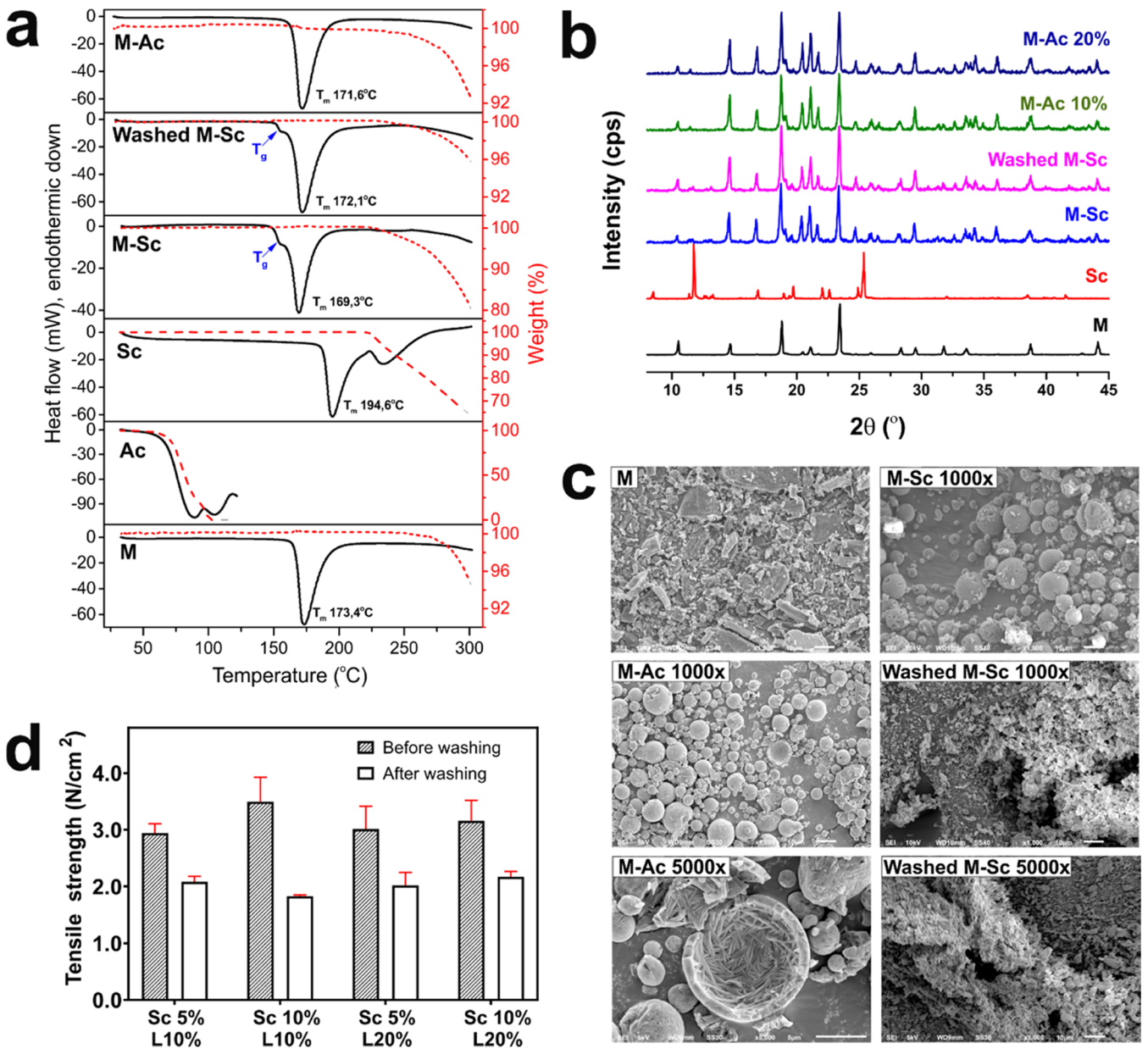

Figure 2. Thermograms of mannitol (M), ammonium carbonate (Ac), sucrose (Sc), and mesoporous mannitol (M-Sc or M-Ac) (heat flow, blank line; weight, red dashed line) (a), diffractogram of mannitol and mesoporous mannitol (b), scanning electron microscopy photograph of mannitol mesoporous (c), and the effect of elimination of templating agent on tensile strength on the spray-dried M-Sc (d).

solidification.[10] Preconcentrated SNE was prepared by mixing all components and stirring at 300 rpm overnight. An excess of PVT (150 mg/mL) was added to the SNE formulation. In order to achieve an equilibrium state at 25 ± 2 °C, it was stirred at 100 rpm for 72 h, followed by centrifugation at 15,000*g*. The supernatant was separated and stored at a controlled temperature of 26 ± 1 °C until the solidification process was performed.

The incorporation of SSNE into the carrier was carried out by using an adsorption mechanism. The SSNE concentration in the final mixture was a fixed amount of 20% (v/w). Solidification was performed by mixing SSNE and mannitol mesoporous to achieve solid SSNE (sSSNE). The sSSNE was stored in a desiccator until further evaluation.

2.10. Characterization of Solid Supersaturable Self-Nanoemulsion. Flowability of sSSNE was characterized by using an angle of repose and compressibility index. A total of 50 g of sSSNE was passed through an orifice with an opening diameter of 12 mm. The powder was allowed to flow, and the diameter (d) and height (h) of the powder pile were measured accurately using a caliper (accuracy of 0.01 mm). The angle of repose (AoR) was calculated according to the following equation

$$\tan(\mathrm{AoR}) = \frac{2h}{d} \tag{3}$$

Meanwhile, the compressibility index was determined using an Erweka tapping device. A 50 g of sSSNE was placed into 100 mL of a volumetric flask, and initial volume (V_o) was noted. The volumetric flask was placed on a tapping device and tapped 500 times. Volume after tapping (V_t) was measured, and the compressibility index could be calculated according to the following equation

https://doi.org/10.1021/acsomega.3c05948
ACS Omega 2023, 8, 38676−38689

$$\text{compressibility index} = \frac{V_t}{V_o} \times 100\% \quad (4)$$

Drug release was evaluated using an Erweka DT-820 dissolution tester (Heusenstamm, Germany) with type II (paddle). A 900 mL aliquot of SGF at pH 1.2 was used as a medium, and then temperature and agitation were controlled at 37 ± 0.5 °C and 50 rpm. The tablet was placed in a 316 L wired sinker (diameter and length of 20 and 35 mm, respectively) and introduced into each dissolution vessel. The sample was withdrawn at predetermined times, 0.08, 0.25, 0.5, 1.0, 1.5, 2.0, 3.0, 4.0, 5.0, 6.0, and 7.0 h. Furthermore, the sample was analyzed spectrophotometrically at a wavelength of 232 nm by a validated analytical method.

2.11. Optimization and Characterization of Optimized Formulation. Optimized formulation was determined by the overlay function of several parameters, i.e., flow characteristics, compaction behavior, pore formation, and drug release parameters. Each parameter had critical priority and limitation, presented in Table S2 (Supporting Data). Each parameter response was overlaid to obtain the superimposed region that depicts the optimized region. In order to verify the optimized formulation, the statistical analysis was based on a *t*-test along with a 95% confidence level.

The optimized sSSNE formulation was characterized by the aforementioned methods by crystallinity through PXRD, nanodroplet formulation using dynamic light scattering (DLS), and sorption−desorption kinetics using BET analysis.

3. RESULTS AND DISCUSSION

3.1. Preparation of Mannitol Mesoporous. Mesoporous mannitol was prepared using the spray-drying technique along with two different templating agents, sucrose and ammonium carbonate. In order to eliminate the TA, particularly for mannitol-sucrose mesoporous material, washing with ethanol was carried out. Sucrose is soluble in ethanol, but mannitol has a solubility limitation in ethanol.[26] According to the characteristics, it was applied to eliminate sucrose from spray-dried mannitol. Conversely, ammonium carbonate has a low decomposition temperature, around 70−100 °C.[27] Therefore, the inlet temperature in the spray-drying process could be applied to eliminate TA from the spray-dried mannitol simultaneously. In order to ensure the mesoporous preparation process for the elimination of TA, several characterizations were carried out, e.g., thermal behavior (Figure 2a), crystallinity (Figure 2b), morphology (Figure 2c), and compaction behavior (Figure 2d).

The thermograms of mannitol, TAs, and treated mesoporous mannitol are presented in Figure 2a. Mannitol has a specific endothermic phenomenon, i.e., melting at 173.4 °C along with decomposition starting at 270 °C, and it decomposed about 6% until 300 °C. Meanwhile, ammonium carbonate started to decompose at 40 °C, and it significantly reduced its weight at 68 °C, followed by completely disappearing at 100 °C. In addition, sucrose has different characteristics of thermal behavior. The melting point of sucrose was higher than that of mannitol, i.e., 194.6 °C, along with weight loss starting from 218 °C, and it was decomposed about 35% while it was heated until 300 °C. Spray-dried mannitol-sucrose (M-Sc) showed a unique characteristic, i.e., small glass transition temperature owing to the amorphous form of mannitol spray dried. The amorphous state formation is affected by the presence of sucrose. Thereafter, the endothermic transition owing to mannitol was observed at 169.3 °C. It had a similar enthalpy value to mannitol, but shifting to the lower melting temperature was observed. In addition, weight loss was observed at 210 °C due to sucrose's presence in this system and its decomposition. Comparable to the washed M-Sc, the thermal behavior around the mannitol melting point had no significant alteration. Meanwhile, the melting peak was observed at 172.1 °C along with no decomposition around 210 °C. Therefore, it indicated that ethanol washing could eliminate TA. It was strengthened by the weight loss of about 5%; thus, it pointed out the characteristics of pure mannitol. However, the enthalpy of the glass transition was altered when sucrose was eliminated from the system. The washing process promoted a lower enthalpy of T_g. Thus, it can be concluded that sucrose interacted with mannitol in an amorphous form. The mannitol-ammonium carbonate spray-dried has no significant difference from pure mannitol, along with a melting peak at 171.6 °C and decomposition at about 7% (until 300 °C).

The diffractogram of mannitol and mannitol spray dried is presented in Figure 2b. Mannitol and sucrose had different specific peaks. All spray-dried mannitol formulations had a broadening peak owing to an amorphous formation and a similar pattern and distinct intensities. The sucrose peak disappeared due to its quantity and dispersed molecularly. This result strengthened the thermal analysis that sucrose dispersed homogeneously in the mannitol spray dried. New peaks were observed at diffraction angles of around 17−25°. It was indicated that the spray-dried sample had a different crystal lattice structure. In addition, the washing process (washed M-Sc) has no significant effect on the alteration of the diffractogram. Therefore, the washing process did not alter the packing of the crystal structure. The peak of spray-dried material, along with ammonium carbonate as TA, was narrower than that of sucrose. This result was similar to that of the DSC thermogram.

The morphologies of mannitol and spray-dried mannitol are presented in Figure 2c. Mannitol had a rod-flake shape in an irregular structure. Meanwhile, the spray-dried mannitol had a spherical structure along with a particle size of 0.5−20 μm. The M-Sc had a solid structure both on the surface and core. On the other hand, the M-Ac had a hollow structure in the particle's core and perforated on the surface. The washing process altered the morphological behavior of spray dried and transformed to an irregular shape with perforation on the surface. Those modifications were intended to enhance the specific surface area for the adsorption of liquid SNE into mesoporous mannitol. In addition, the absorption mechanism could be achieved owing to the natural behavior of mannitol characteristics.[12]

Not only the morphological behavior but also the washing process altered the compaction properties. It is depicted in Figure 2d. Sucrose enhanced the compaction ability through the plastic deformation characteristics[28];[28] meanwhile, mannitol has brittle characteristics.[29,30] The higher the sucrose, the greater the tablet strength. Meanwhile, the solid loading had no significant effect on the tensile strength. The solid loading might affect the particle size of the spray-dried mannitol. The higher the loading, the greater the particle size. According to all of those characterizations, the mannitol mesoporous form, either with ammonium carbonate or sucrose as a templating agent, is applicable for solidifying SNE formulation.

3.2. Effect on the Surface Area. The surface area determines the effectiveness of the solidification of SNE formulation.[11] Solidification of SNEDDS using mannitol involves two mechanisms; however, the absorption mechanism is more dominant than the adsorption mechanism. The larger

https://doi.org/10.1021/acsomega.3c05948
ACS Omega 2023, 8, 38676−38689

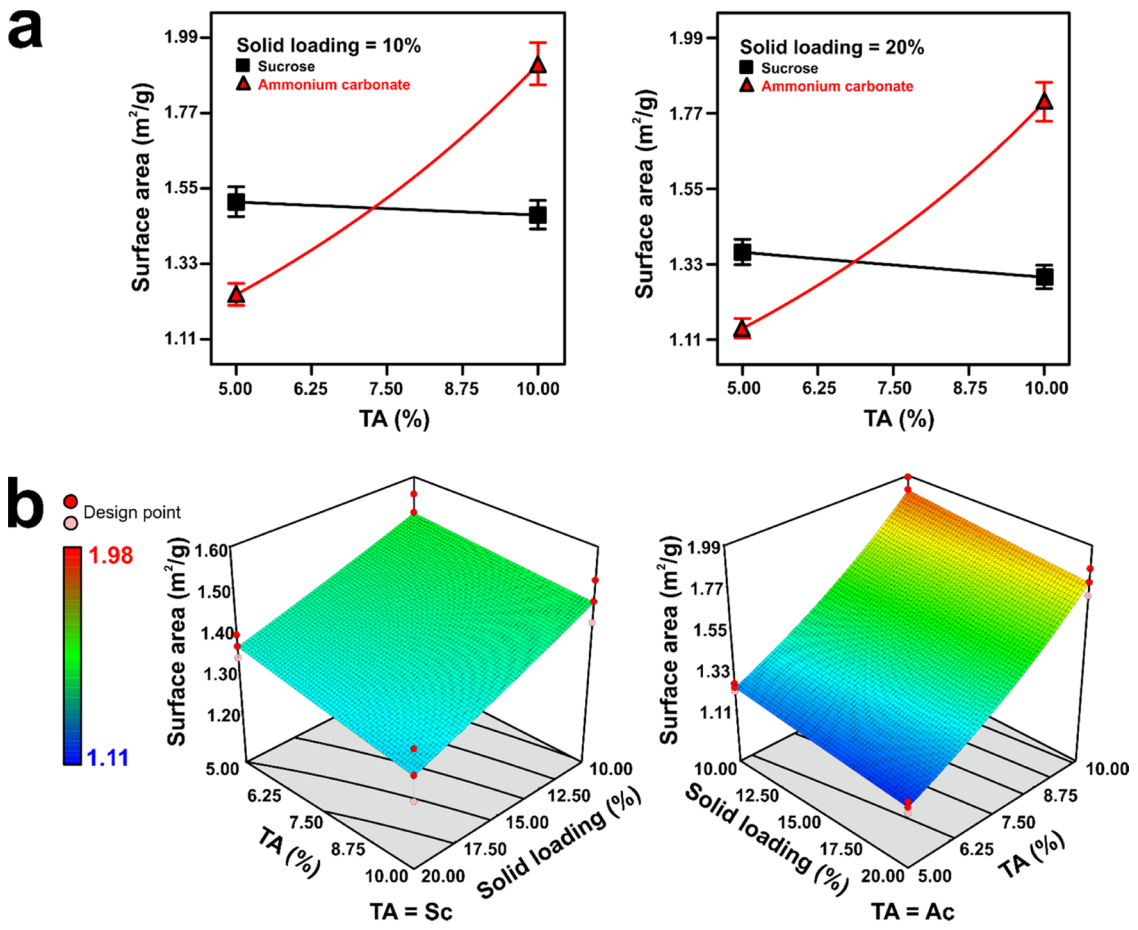

Figure 3. Interaction plot (a) and surface plot (b) of the BET-specific surface area. TA (templating agent), Sc (sucrose), and Ac (ammonium carbonate).

the surface area, the greater the potency of the absorption mechanism.[12]. In this work, the preparation process was studied extensively to elucidate and optimize mesoporous mannitol. The surface area of the modified mannitol was in the range of 1.112−1.981 m^2/g. This elimination of a templating agent for preparing mesoporous material successfully enhanced the surface area of mannitol (mannitol's surface area was 0.593 ± 0.007 m^2/g). Different solid loadings had a pattern similar to the TA concentration on surface area profiles (Figure 3a). Meanwhile, the Ac as TA had no significant effect on different solid loadings. The surface area reduction was observed on the solid loading of 20%, along with Sc as TA. This phenomenon was confirmed by isothermal sorption desorption kinetic profiles (Figure S1, Supporting Data). Therefore, Ac had more potential TA for preparing the mesoporous mannitol according to the surface area.

Based on the factorial analysis (Table 1), all factors significantly affected surface area ($p < 0.05$). The increase of solid loading contributed to the reduction of mannitol mesoporous surface area, while the increase of TA concentration promoted enhancing the surface area of mannitol mesoporous. There was no significant interaction between factors except TA concentration and TA type. The surface plot of the surface area is presented in Figure 3b. Sc had a middle range of surface area; meanwhile, Ac had a broad range of surface area. However, the highest and lowest surface area levels were obtained using Sc as TA. Therefore, the selection of TA and TA concentration had significant consideration for preparing mannitol mesoporous material.

3.3. Effect on Pore Formation. Pore formation behavior was assigned by pore volume and pore size. These data strengthened the surface area parameter for solidifying the liquid preconcentrated nanoemulsion formulation. The larger pore size and pore volume made it easy to incorporate the liquid preconcentrated formulation into mannitol mesoporous.[23] Pore size determines the liquid incorporation rate into mesoporous material, and pore volumes govern the amount of liquid formulation loaded into mesoporous mannitol.[20,22] The pore size and pore volume of mesoporous mannitol were 12.5−310.6 nm and 7.8−65.3 × 10^{-3} cm^3/g, respectively. Different solid loadings on mannitol mesoporous preparation had similar patterns, both Ac and Sc as TA (Figure 4a). However, the pore size was reduced as solid loading increased. Both TAs had a similar pattern. The lower the solid loading, the greater the pore size was at a similar TA level. The surface plot of the pore size (Figure 4b) had a different value between TAs. Sc had a low-to-middle pore size value, while Ac had a middle-to-high pore size value. Hence, Ac had more significant consideration for preparing the more porous material than Sc regarding the effectiveness of the pore formation. The pore volume formation was similar to that of the pore size data (Figure 4c,d).

3.4. Effect on Tensile Strength. The particle bonding strength due to the applied force is depicted by the tensile strength. For further process, solids can be prepared in solid and compact formulations, e.g., tablets.[31] Therefore, this evaluation

https://doi.org/10.1021/acsomega.3c05948
ACS Omega 2023, 8, 38676−38689

Table 1. Regression Coefficient and Fitting Parameters Model of Responses Using Factorial Design[a,b,c]

	$(Y_1)^{-1/2}$ (m^3/g)		$\log(Y_2)$ (nm)		$\log(Y_3)$ (mL/g)		Y_4 (N/cm^2)		Y_5 (deg)		Y_6 (%)		Y_7 (%)		Y_8 (%)	
parameters	CR	p	CR	p	CR	p	CR	p	CR	p	CR	p	CR	p	CR	p
intercept	0.83		1.61		1.22		2.26		33.71		20.71		52.12		75.59	
A	0.02	0.000	−0.2	0.000	0.005	0.007	0.14	0.000	0.046	0.895	0.36	0.485	1.76	0.011	1.27	0.069
B	−0.041	0.000	0.11	0.000	−0.14	0.000	0.25	0.000	0.093	0.789	−1.94	0.001	−2.78	0.001	−0.011	0.987
C	−0.009	0.005	0.062	0.010	0.29	0.000	0.2	0.000	−2.8	<0.001	−38	<0.001	8.5	<0.001	5.28	<0.001
AB	−0.001	0.905	−0.17	0.000	0.01	0.000	−0.13	0.001	0.59	0.104	0.47	0.361	0.12	0.852	0.06	0.928
AC	−0.005	0.099	−0.09	0.001	0.033	0.000	0.24	0.000	−0.05	0.886	1.14	0.037	0.047	0.941	−1.09	0.114
BC	−0.05	0.000	−0.041	0.067	−0.13	0.000	0.26	0.000	0.12	0.732	−0.081	0.873	−1.79	0.012	0.24	0.722
ABC	−0.004	0.203	−0.13	0.000	0.004	0.04	−0.02	0.654	−0.8	0.032	−0.082	0.871	−2.49	0.001	−1.64	0.023
p	0.000		0.000		0.000		0.000		0.000		0.000		0.000		0.000	
R^2	0.975		0.9406		0.9996		0.9462		0.8253		0.8083		0.9382		0.932	
adjusted R^2	0.964		0.9145		0.9995		0.9226		0.7489		0.7244		0.9112		0.859	
predicted R^2	0.9437		0.8662		0.9992		0.8789		0.6070		0.5687		0.8610		0.6222	
AP	27.3		19.86		189.59		20.45		7.73		9.8		17.8		8.98	

[a] A, solid loading (%); B, TA (%); C, type of TA. [b] CR, coefficient of regression; p, p-value; Y_1, surface area; Y_2, pore size; Y_3, pore volume; Y_4, tensile strength; Y_5, angle of repose; Y_6, compressibility index; Y_7, drug release at 5 min; and Y_8, dissolution efficiency during 30 min. [c] R^2 = determination coefficient; adj. R^2, adjusted R^2; pred. R^2, predicted R^2; adeq prec., adequate precision.

was intended to characterize the compaction ability of sSSNE under a predetermined applied force. Prior to evaluation, sSSNE was prepared according to the previous method, i.e., 20% preconcentrated liquid SNE formulation incorporated into mesoporous mannitol. Our previous work revealed that solidifying SNE formulation into mesoporous material did not alter the porous behavior.[12] Therefore, different porous structures of mesoporous material might alter the compaction behavior of mannitol mesoporous. The tensile strength of mannitol mesoporous was considerably high in the range of 1.30−3.35 N/cm^2.

The templating agent concentration had the most excellent effect on affecting the increase of tensile strength (Table 1). Different templating agent concentrations, 5 and 10% (Figure 5a), had different patterns. In low concentrations of TA (5%), the tensile strength of mannitol mesoporous along with sucrose as TA had an insignificant alteration with increasing solid loading. Meanwhile, a distinct pattern was observed at higher concentrations (10%). The tensile strength dropdown with the increase of solid loading. The solid loading mainly affected particle size formation. The greater the solid loading, the smaller the particle size. Sc and Ac had different and unique patterns on the surface plot (Figure 5b). At a high level of solid loading (20%) and TA concentration (10%), the tensile strength of the Ac mesoporous material was higher than that of Sc. Meanwhile, the low level of solid loading (10%) and TA, mannitol mesoporous, and Ac as TA were the lowest tensile strength. This phenomenon was affected by the material's pore; the larger the pore volume, the lower the tensile strength. The entrapped air in the compacted material promotes reducing the interparticle bonding.[32] Hence, the tensile strength dropped down. However, this result was consistent with the surface area. The surface area is involved in the contribution of interparticle bonding.

3.5. Effect on Flowability. The flowability implies the flow characteristics of sSSNE. In the study, the flowability was measured according to the angle of repose and compressibility index.[33] The angle of repose for all SSNE formulations was in the range of 29.09−39.75°. According to the USP, it was categorized as good-to-fair (not aid required) flow characteristics.[34] Meanwhile, Carr's index was 13.33−29.17%, categorized as having good-to-poor flow characteristics. An opposite pattern was observed in the interaction plot of the angle of repose, particularly Sc as a TA (Figure 6a). However, Sc had no significant changes in the angle of repose as altering the solid loading under different amounts of TA ($p > 0.05$). sSSNE prepared using mesoporous material along with Ac as TA had better powder flow than material mesoporous with Sc as TA. It was proven by the surface plot of the angle of repose (Figure 6b). On the other side, the flow characteristics seen by Carr's index had somewhat similar sounds to the angle of repose. The interaction plot of Carr's index (Figure 6c) showed that the TA concentration affected Carr's index. Meanwhile, the solid loading did not significantly affect Carr's index ($p > 0.05$). All sSSNEs using Ac as TA had good-to-fair flow characteristics. Meanwhile, the sSSNE using Sc as TA had poor flow characteristics. The surface plot profile of Carr's index (Figure 6d) showed that the poorest flow characteristic was observed at a low level of solid loading (10%) and TA concentration (5%) using Sc as TA. Meanwhile, the best flow characteristic was observed at the low level of solid loading (10%) and high TA concentration (10%). Those data showed good flowability when sSSNE was prepared using mannitol mesoporous with Ac as TA.

https://doi.org/10.1021/acsomega.3c05948
ACS Omega 2023, 8, 38676−38689

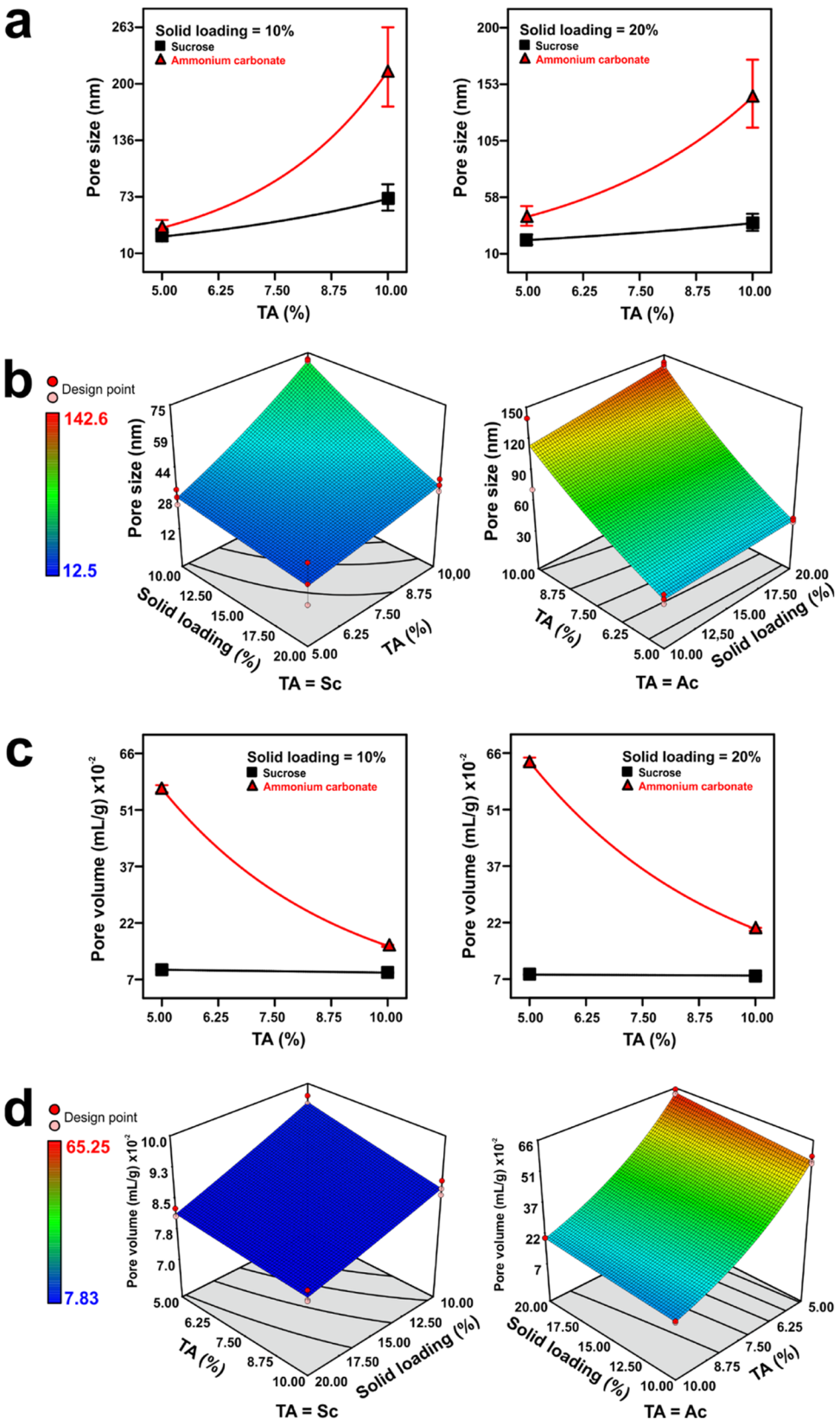

Figure 4. Interaction (a) and surface (b) plots of pore size, and interaction (c) and surface (d) plots of pore volume. TA (templating agent), Sc (sucrose), and Ac (ammonium carbonate).

This result was affected by the shape behavior. According to the preparation data, the mesoporous material prepared by Ac as TA achieved spherical particles with a hollow structure. Therefore, the efficient solidification was due to pore formation due to liquid and high cohesiveness value, and the presence of SSNE on the surface of mannitol mesoporous reduced flowability.[33]

https://doi.org/10.1021/acsomega.3c05948
ACS Omega 2023, 8, 38676−38689

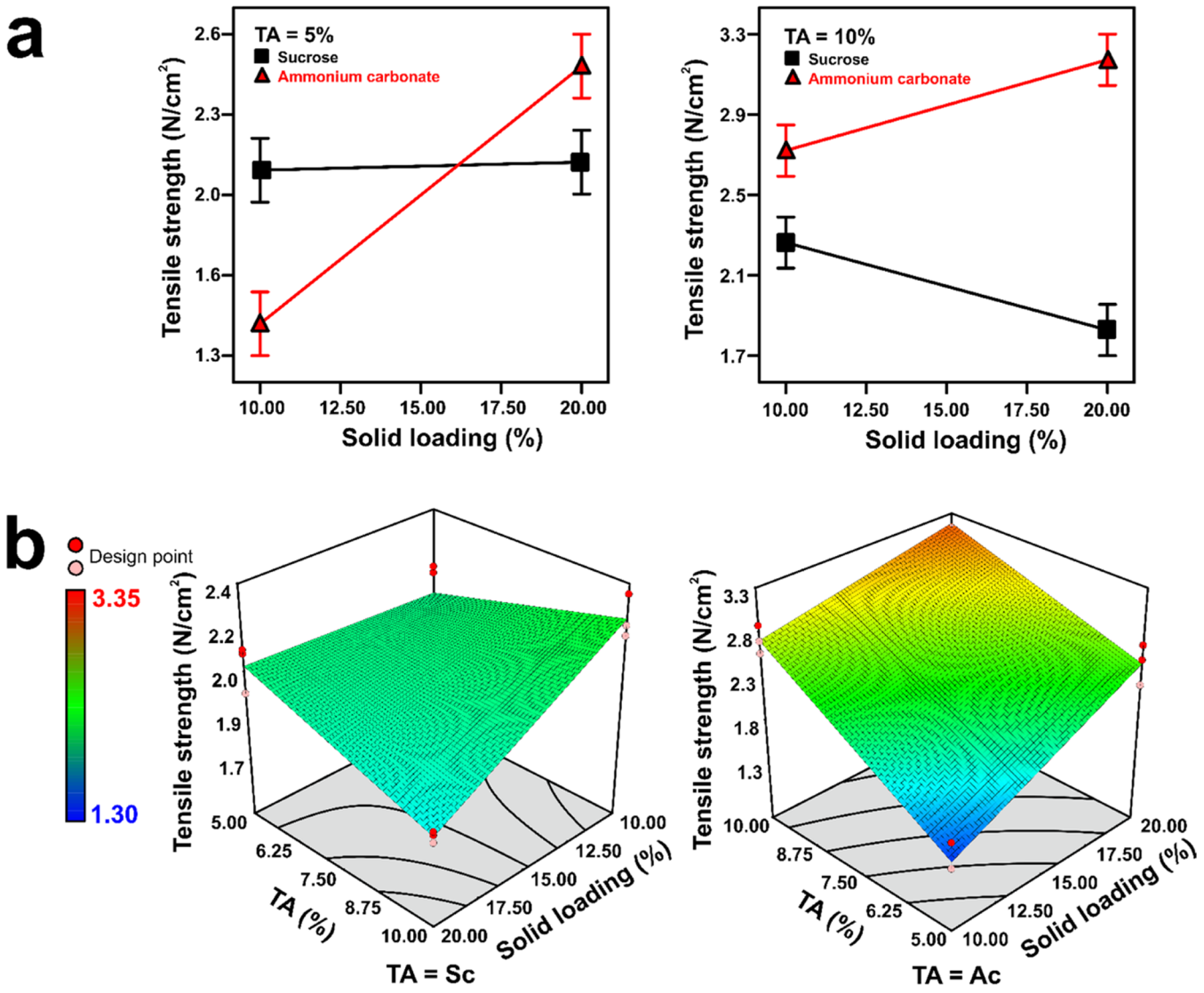

Figure 5. Interaction (a) and surface (b) plots of the tensile strength. TA (templating agent), Sc (sucrose), and Ac (ammonium carbonate).

3.6. Effect on Drug Release. The drug release in this study depicted the nanodroplet formation of sSSNE when introduced into the medium.[11,35] The lipophilic drug is still entrapped in the oily droplets; however, the nanodroplet was released when the mannitol mesoporous dissolved. Therefore, the drug release response mimics the formation of nanodroplets. Owing to the soluble characteristics of mannitol, it would be easier to dissolve when it was introduced into the water, followed by a self-emulsifying mechanism.[12,20] Drug release profiles of sSSNE using Sc and Ac as TAs are presented in Figure 7a,7b, respectively. The drug release profile was different, particularly in the early times. The sSSNE prepared by using Ac as TA was completely dissolved for 10 min. Meanwhile, complete dissolution of the sSSNE prepared using Sc as TA was found at 30 min. This phenomenon was caused by a different crystal lattice structure. The higher the amorphous crystal structure of mannitol mesoporous, the easier it is to dissolve.[18,26] In order to evaluate the drug release profile, a one-point method according to the drug release at 5 min due to the inflection point of the drug release profile was selected. In addition, the multiple-point method was applied to compare the drug release profile and the relative area under the curve of drug release during 10 min, DE_{30min}.

According to the interaction plot of the Q_{5min} parameter (Figure 7c), the solid loading was affected by the pattern of Q_{5min}. Solid loading, amount of TA, and TA type were significantly affected by the Q_{5min} ($p < 0.05$). A blatant interaction was observed at low and high levels of concentration of TA under different solid loadings, particularly at sSSNE prepared using Ac. The surface plot of Q_{5min} (Figure 7d) showed that the Q_{5min} of sSSNE Ac-based mesopores was higher than that of Sc. The highest Q_{5min} was obtained at a low level of PPA (5%) and a high level of solid loading (20%); meanwhile, the lowest Q_{5min} was observed at a high level of TA (10%) and low level of solid loading (10%). A different point of view on drug release was evaluated according to the multiple-point comparison. The interaction plot of DE_{10min} (Figure 7e) implied that there was no significant difference related to the solid loading and TA amount on the DE_{10min} ($p > 0.05$). However, the alteration of TA type significantly affected DE_{10min} ($p < 0.05$). The surface plot of DE_{10min} (Figure 7f) confirmed this phenomenon; i.e., only the TA type affected the whole drug release profile. Generally, both formulations based on Ac and Sc

https://doi.org/10.1021/acsomega.3c05948
ACS Omega 2023, 8, 38676−38689

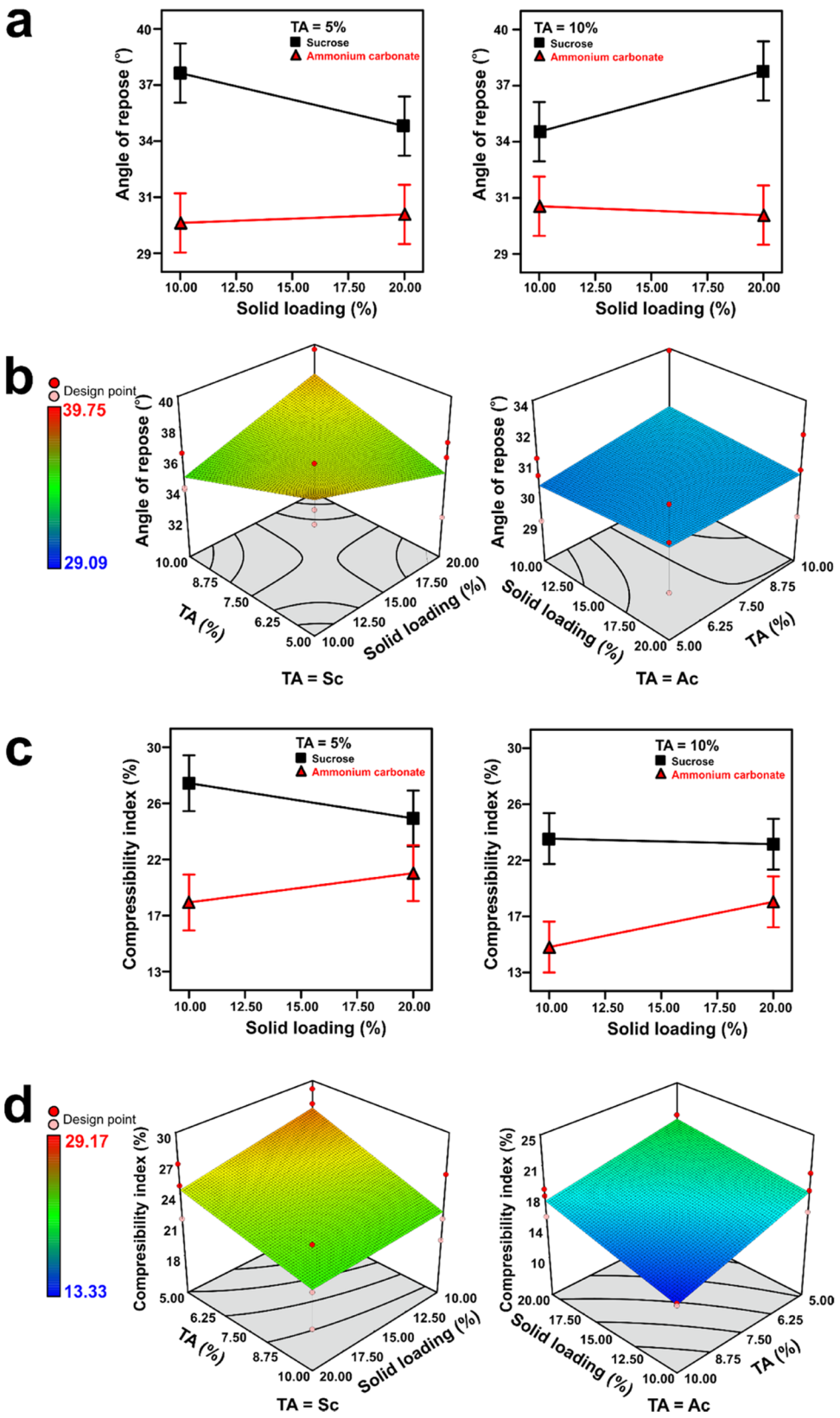

Figure 6. Interaction (a) and surface (b) plots of the angle of repose, and interaction (c) and surface (d) plots of compressibility index. TA (templating agent), Sc (sucrose), and Ac (ammonium carbonate).

mannitol mesoporous had high drug release (>80% during 10 min). This result faced a potential candidate for bioavailability enhancement of poorly water-soluble pitavastatin.

3.7. Optimization and Nanodroplet Formation. In order to determine the optimized formulation, quality target product profiles of sSSNE pitavastatin are presented in Table S2 (Supporting Information). Drug release gained more priority

https://doi.org/10.1021/acsomega.3c05948
ACS Omega 2023, 8, 38676−38689

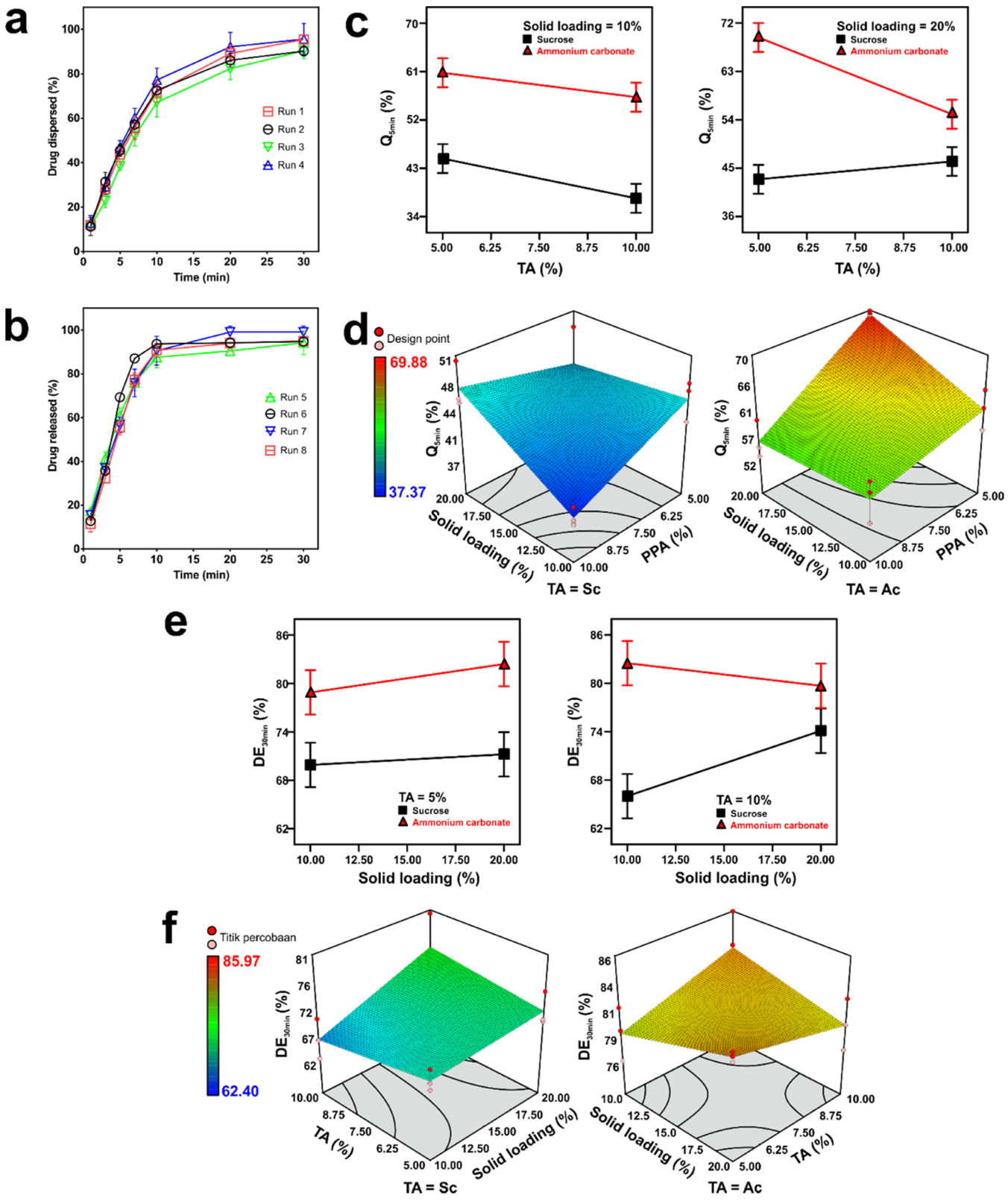

Figure 7. Release profile of sSSNE using mannitol-sucrose (a) and mannitol-ammonium carbonate (b), interaction (c) and surface (d) plots of drug release at 5 min (Q_{5min}), and interaction (e) and surface (f) plots of dissolution efficiency during 30 min (DE_{30min}). TA (templating agent), Sc (sucrose), and Ac (ammonium carbonate).

than other characteristics, e.g., pore formation and compatibility, due to its significant effect on performance for bioavailability enhancement.[22,36] The optimization process used the overlaid plot to obtain the desirability value (Figures S2 and S3, Supporting Information). Therefore, the optimized mesoporous material process was achieved at a solid loading of 20 and 7% Ac as TA. Evaluation of optimized sSSNE was carried out regarding the crystallinity and nanodroplet formation as well as the pore

https://doi.org/10.1021/acsomega.3c05948
ACS Omega 2023, 8, 38676−38689

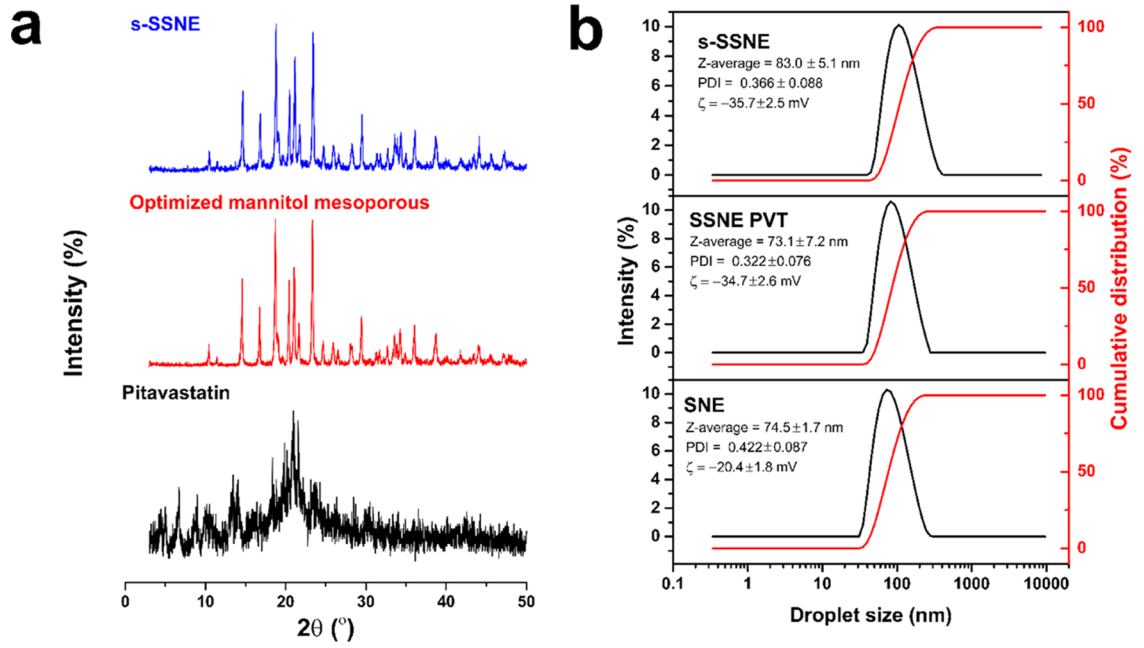

Figure 8. Diffractograms of pitavastatin, optimized mesoporous mannitol, and solid SSNE (sSSNE) (a) and particle size distribution of SNE, SSNE pitavastatin (SSNE PVT), and sSSNE (b).

alteration. The diffractograms of pitavastatin, optimized mesoporous mannitol, and sSSNE are presented in Figure 8a. Pitavastatin had an amorphous structure; meanwhile, optimized mesoporous had a semicrystalline structure due to the broadening of peak compared with the native mannitol diffractogram. sSSNE had a similar diffractogram pattern as well as its specific peak. Meanwhile, the noise peak of the amorphous structure was more intensive in the sSSNE diffractogram. It is due to the presence of absorbed liquid into mesoporous material. The nanodroplet formation was also evaluated in order to investigate the interaction of mesoporous mannitol and liquid preconcentrated SNE formulation. The droplet size distribution profiles of SNE, SSNE PVT, and sSSNE are presented in Figure 8b. The pattern of all curves was in the monodisperse system along with a narrow distribution curve (polydispersity index, PDI < 0.5) [7]. This result proved that there was no alteration of droplet formation regarding the self-nanoemulsion mechanism during the dissolving of the carrier. The droplet size of SNE, PVT-loaded SSNE, and sSSNE was insignificantly different ($p > 0.05$). Therefore, the solidification did not affect the droplet formation. Regarding the droplet stability, the ζ-potential was considerably high enough for repulsion of each other due to less than −25 mV.

4. CONCLUSIONS

The effect of the preparation process of mesoporous material on the solidification of SNE was successfully and simultaneously assessed using a 2^3-factorial design. Several process parameters for preparing the mesoporous mannitol gained more significant consideration, notably TA. Switching from mannitol to ammonium carbonate as the templating agent had better performance as the carrier for solidifying SNE. Solid loading in the mesoporous preparation system promoted the reduction of surface area and pore size, increased the pore volume, and had no effect on sSSNE flowability. The amount of TA increased the pore size and volume significantly, as well as the compactibility and flowability. Ammonium carbonate was the preferable TA for preparing the mesoporous carrier, particularly for the nanodroplet formulation process. Both synergistic and antagonistic interactions were observed in affecting the performance of mesoporous carriers for solidification. The optimized mesoporous carrier consisted of 7% ammonium carbonate and 20% total solid loading. The optimized mesoporous carrier proved that there was no difference between SSNE and sSSNE in the performance of nanodroplet formation. Moreover, precipitation during dilution was also not observed.

■ ASSOCIATED CONTENT

Data Availability Statement

The data sets used and analyzed in this study can be obtained from the corresponding authors in combination with specific and reasonable requirements.

Supporting Information

The Supporting Information is available free of charge at https://pubs.acs.org/doi/10.1021/acsomega.3c05948.

Design of experiment of mannitol mesoporous preparation; quality target product profile, and desirability for determination of the optimized formulation and N_2 isothermal sorption desorption kinetics of mesoporous mannitol (PDF)

■ AUTHOR INFORMATION

Corresponding Author

Syaiful Choiri − *Pharmaceutical Technology and Drug Delivery, Department of Pharmacy, Universitas Sebelas Maret, Surakarta 57126, Indonesia;* orcid.org/0000-0001-7750-6008; Email: s.choiri@mipa.uns.ac.id

Authors

Ilham Kuncahyo − *Faculty of Pharmacy, Setia Budi University, Surakarta 57127, Indonesia*

Ana Indrayati − *Faculty of Pharmacy, Setia Budi University, Surakarta 57127, Indonesia*

https://doi.org/10.1021/acsomega.3c05948
ACS Omega 2023, 8, 38676−38689

Complete contact information is available at:
https://pubs.acs.org/10.1021/acsomega.3c05948

Author Contributions

Conceptualization, S.C. and I.K.; methodology, S.C.; software, S.C.; validation, all authors; formal analysis, S.C.; investigation, I.K. and A.I.; resources, S.C.; data curation, I.K.; writing—original draft preparation, I.K.; writing—review and editing, S.C.; visualization, S.C.; supervision, S.C.; project administration, A.I.; and funding acquisition, I.K.

Funding

This research was funded by the Ministry of Education, Culture, Research, and Technology, the Republic of Indonesia, along with contract Nos. 036/E5/PG.02.00/2022 and 001/LL6/PB2/AK.04/2022.

Notes

The authors declare no competing financial interest.

■ ACKNOWLEDGMENTS

The authors would like to thank the Ministry of Education, Culture, Research, and Technology, Republic of Indonesia and Universitas Sebelas Maret for funding and supporting this research, respectively.

■ REFERENCES

(1) Holm, R. Bridging the Gaps between Academic Research and Industrial Product Developments of Lipid-Based Formulations. *Adv. Drug Delivery Rev.* **2019**, *142*, 118−127.
(2) Huang, Y.; Yu, Q.; Chen, Z.; Wu, W.; Zhu, Q.; Lu, Y. In Vitro and in Vivo Correlation for Lipid-Based Formulations: Current Status and Future Perspectives. *Acta Pharm. Sin. B* **2021**, *11* (8), 2469−2487.
(3) Savić, V.; Ilić, T.; Nikolić, I.; Marković, B.; Čalija, B.; Cekić, N.; Savić, S. Tacrolimus-Loaded Lecithin-Based Nanostructured Lipid Carrier and Nanoemulsion with Propylene Glycol Monocaprylate as a Liquid Lipid: Formulation Characterization and Assessment of Dermal Delivery Compared to Referent Ointment. *Int. J. Pharm.* **2019**, *569*, No. 118624.
(4) Khatri, P.; Shao, J. Mechanism and Structural Factors of Lipid and Surfactant in the Formation of Self-Emulsified Nanoemulsion. *J. Pharm. Sci.* **2018**, *107* (8), 2198−2207.
(5) Phan, T. N. Q.; Shahzadi, I.; Bernkop-Schnürch, A. Hydrophobic Ion-Pairs and Lipid-Based Nanocarrier Systems: The Perfect Match for Delivery of BCS Class 3 Drugs. *J. Controlled Release* **2019**, *304*, 146−155.
(6) Shah, D.; Guo, Y.; Ban, I.; Shao, J. Intranasal Delivery of Insulin by Self-Emulsified Nanoemulsion System: In Vitro and in Vivo Studies. *Int. J. Pharm.* **2022**, *616*, No. 121565.
(7) Yao, M.; Li, Z.; McClements, D. J.; Tang, Z.; Xiao, H. Design of Nanoemulsion-Based Delivery Systems to Enhance Intestinal Lymphatic Transport of Lipophilic Food Bioactives: Influence of Oil Type. *Food Chem.* **2020**, *317*, No. 126229.
(8) Celli, G. B.; Liu, Y.; Dadmohammadi, Y.; Tiwari, R.; Raghupathi, K.; Mutilangi, W.; Abbaspourrad, A. Instantaneous Interaction of Mucin with Pectin- and Carrageenan-Coated Nanoemulsions. *Food Chem.* **2020**, *309*, No. 125795.
(9) Zaichik, S.; Steinbring, C.; Jelkmann, M.; Bernkop-Schnürch, A. ζ-potential Changing Nanoemulsions: Impact of PEG-Corona on Phosphate Cleavage. *Int. J. Pharm.* **2020**, *581*, No. 119299.
(10) Kuncahyo, I.; Choiri, S.; Fudholi, A.; Martien, R.; Rohman, A. Development of Pitavastatin-Loaded Super-Saturable Self-Nano Emulsion: A Continues Screening and Optimization Approach Using Statistical Technique. *J. Dispersion Sci. Technol.* **2023**, *44* (4), 608−617.
(11) Almeida, S. R. D.; Tippavajhala, V. K. A Rundown Through Various Methods Used in the Formulation of Solid Self-Emulsifying Drug Delivery Systems (S-SEDDS). *AAPS PharmSciTech* **2019**, *20* (8), No. 323.
(12) Kuncahyo, I.; Choiri, S.; Fudholi, A. Solidification of Meloxicam Self-Nano Emulsifying Drug Delivery System Formulation Incorporated into Soluble and Insoluble Carriers Using Freeze Drying Method. *IOP Conf. Ser.: Mater. Sci. Eng.* **2019**, *578*, No. 012051, DOI: 10.1088/1757-899X/578/1/012051.
(13) Kang, J. H.; Oh, D. H.; Oh, Y.-K.; Yong, C. S.; Choi, H.-G. Effects of Solid Carriers on the Crystalline Properties, Dissolution and Bioavailability of Flurbiprofen in Solid Self-Nanoemulsifying Drug Delivery System (Solid SNEDDS). *Eur. J. Pharm. Biopharm.* **2012**, *80* (2), 289−297.
(14) Møller, A.; Schultz, H. B.; Meola, T. R.; Müllertz, A.; Prestidge, C. A. The Influence of Solidification on the in Vitro Solubilisation of Blonanserin Loaded Supersaturated Lipid-Based Oral Formulations. *Eur. J. Pharm. Sci.* **2021**, *157*, No. 105640.
(15) Sharma, P.; Singh, S. K.; Pandey, N. K.; Rajesh, S. Y.; Bawa, P.; Kumar, B.; Gulati, M.; Singh, S.; Verma, S.; Yadav, A. K.; Wadhwa, S.; Jain, S. K.; Gowthamarajan, K.; Malik, A. H.; Gupta, S.; Khursheed, R. Impact of Solid Carriers and Spray Drying on Pre/Post-Compression Properties, Dissolution Rate and Bioavailability of Solid Self-Nanoemulsifying Drug Delivery System Loaded with Simvastatin. *Powder Technol.* **2018**, *338*, 836−846.
(16) Pomázi, A.; Ambrus, R.; Sipos, P.; Szabó-Révész, P. Analysis of Co-Spray-Dried Meloxicam−Mannitol Systems Containing Crystalline Microcomposites. *J. Pharm. Biomed. Anal.* **2011**, *56* (2), 183−190.
(17) Saffari, M.; Ebrahimi, A.; Langrish, T. Nano-Confinement of Acetaminophen into Porous Mannitol through Adsorption Method. *Microporous Mesoporous Mater.* **2016**, *227*, 95−103.
(18) Saffari, M.; Ebrahimi, A.; Langrish, T. Highly-Porous Mannitol Particle Production Using a New Templating Approach. *Food Res. Int.* **2015**, *67*, 44−51.
(19) Ebrahimi, A.; Saffari, M.; Langrish, T. Improving the Dissolution Rate of Hydrophobic Drugs through Encapsulation in Porous Lactose as a New Biocompatible Porous Carrier. *Int. J. Pharm.* **2017**, *521* (1), 204−213.
(20) Kuncahyo, I.; Choiri, S.; Fudholi, A.; Rohman, A.; Martien, R. Understanding the Effect of Lipid Formulation Loading and Ethanol as a Diluent on Solidification of Pitavastatin Super-Saturable SNEDDS Using Factorial Design Approach. *Res. Pharm. Sci.* **2019**, *14* (5), 378−390.
(21) Kim, J. S.; Choi, Y. J.; Woo, M. R.; Cheon, S.; Ji, S. H.; Im, D.; ud Din, F.; Kim, J. Oh.; Youn, Y. S.; Oh, K. T.; Lim, S.-J.; Jin, S. G.; Choi, H.-G. New Potential Application of Hydroxypropyl-β-Cyclodextrin in Solid Self-Nanoemulsifying Drug Delivery System and Solid Dispersion. *Carbohydr. Polym.* **2021**, *271*, No. 118433.
(22) Kim, D. S.; Yang, E. S.; Yong, C. S.; Youn, Y. S.; Oh, K. T.; Li, D. X.; Kim, J. O.; Jin, S. G.; Choi, H.-G. Effect of Inorganic Mesoporous Carriers on 1-Palmitoyl-2-Linoleoyl-3-Acetyl-Rac-Glycerol-Loaded Solid Self-Emulsifying Drug Delivery System: Physicochemical Characterization and Bioavailability in Rats. *Colloids Surf., B* **2017**, *160*, 331−336.
(23) Riikonen, J.; Xu, W.; Lehto, V.-P. Mesoporous Systems for Poorly Soluble Drugs − Recent Trends. *Int. J. Pharm.* **2018**, *536* (1), 178−186.
(24) Ainurofiq, A.; Hidayat, Y.; Lestari, E. Y. P.; Kumalasari, M. M. W.; Choiri, S. Resveratrol Nanocrystal Incorporated into Mesoporous Material: Rational Design and Screening through Quality-by-Design Approach. *Nanomaterials* **2022**, *12* (2), No. 214.
(25) Ainurofiq, A.; Choiri, S. Development and Optimization of a Meloxicam/β-Cyclodextrin Complex for Orally Disintegrating Tablet Using Statistical Analysis. *Pharm. Dev. Technol.* **2018**, *23* (5), 464−475.
(26) Su, W.; Liu, J.; Wang, H.; Li, C.; Jia, N. Thermodynamic Study of Three Anhydrous Polymorphs of D-Mannitol in Different Binary Solvent Mixtures from T = (258.15 to 278.15) K. *J. Chem. Thermodyn.* **2020**, *141*, No. 105680.
(27) Mohan, S.; Dinesha, P. Thermal Dissociation Kinetics of Solid Ammonium Carbonate for Use in NH3-SCR Systems. *Chem. Pap.* **2022**, *76* (10), 6551−6556.
(28) López-Córdoba, A.; Matera, S.; Deladino, L.; Hoya, A.; Navarro, A.; Martino, M. Compressed Tablets Based on Mineral-Functionalized

Starch and Co-Crystallized Sucrose with Natural Antioxidants. *J. Food Eng.* **2015**, *146*, 234−242.
(29) Tarlier, N.; Soulairol, I.; Bataille, B.; Baylac, G.; Ravel, P.; Nofrerias, I.; Lefèvre, P.; Sharkawi, T. Compaction Behavior and Deformation Mechanism of Directly Compressible Textured Mannitol in a Rotary Tablet Press Simulator. *Int. J. Pharm.* **2015**, *495* (1), 410−419.
(30) Tarlier, N.; Soulairol, I.; Sanchez-Ballester, N.; Baylac, G.; Aubert, A.; Lefevre, P.; Bataille, B.; Sharkawi, T. Deformation Behavior of Crystallized Mannitol during Compression Using a Rotary Tablet Press Simulator. *Int. J. Pharm.* **2018**, *547* (1), 142−149.
(31) Yohannes, B.; Abebe, A. Determination of Tensile Strength of Shaped Tablets. *Powder Technol.* **2021**, *383*, 11−18.
(32) Wang, L. G.; Omar, C.; Litster, J. D.; Li, J.; Mitchell, N.; Bellinghausen, S.; Barrasso, D.; Salman, A.; Slade, D. Tableting Model Assessment of Porosity and Tensile Strength Using a Continuous Wet Granulation Route. *Int. J. Pharm.* **2021**, *607*, No. 120934.
(33) Choi, J. E.; Kim, J. S.; Choi, M.-J.; Baek, K.; Woo, M. R.; Kim, J. O.; Choi, H.-G.; Jin, S. G. Effects of Different Physicochemical Characteristics and Supersaturation Principle of Solidified SNEDDS and Surface-Modified Microspheres on the Bioavailability of Carvedilol. *Int. J. Pharm.* **2021**, *597*, No. 120377.
(34) *United States Pharmacopoeia 41-National Formulary 36*; The United States Pharmacopeial Convention: Rockville, Maryland, USA, 2019; 801−804.
(35) Md, S.; Alhakamy, N. A.; Aldawsari, H. M.; Ahmad, J.; Alharbi, W. S.; Asfour, H. Z. Resveratrol Loaded Self-Nanoemulsifying Drug Delivery System (SNEDDS) for Pancreatic Cancer: Formulation Design, Optimization and in Vitro Evaluation. *J. Drug Delivery Sci. Technol.* **2021**, *64*, No. 102555.
(36) Jaisamut, P.; Wanna, S.; Limsuwan, S.; Chusri, S.; Wiwattanawongsa, K.; Wiwattanapatapee, R. Enhanced Oral Bioavailability and Improved Biological Activities of a Quercetin/Resveratrol Combination Using a Liquid Self-Microemulsifying Drug Delivery System. *Planta Med.* **2021**, *87* (4), 336−346.

https://doi.org/10.1021/acsomega.3c05948
ACS Omega 2023, 8, 38676−38689